Journal of the Optical Society of Korea
Vol. 19, No. 4, August 2015, pp. 346-350
ISSN: 1226-4776(Print) / ISSN: 2093-6885(Online)
DOI: http://dx.doi.org/10.3807/JOSK.2015.19.4.346

Measurement of Effective Refractive Index of Nematic Liquid Crystal in Fabry-Perot Etalon

Myeong Ock Ko[1], Sung-Jo Kim[1], Jong-Hyun Kim[1], Bong Wan Lee[2], and Min Yong Jeon[1]*

[1]Department of Physics, Chungnam National University, Daejeon 305-764, Korea
[2]Fiberpro, Daejeon 305-700, Korea

(Received February 25, 2015 : revised June 30, 2015 : accepted June 30, 2015)

We report a measurement of the effective refractive index of a nematic liquid crystal (NLC) inside a Fabry-Perot (FP) etalon according to the applied electric fields. The effective refractive index of the NLC depends on the intensity of the applied electric field. A wavelength-swept laser with a polygon-scanner-based wavelength filter is used as a wide-band optical source to measure the effective refractive index of the NLC. The bandwidth of the optical source is greater than 90 nm around 1300 nm. The fabricated NLC FP etalon consists of glass substrates, gold layers as the electrodes with highly reflective surfaces, polyimide layers as the planar alignment layers, and an LC layer. Furthermore, we measured the Freedericksz transition voltages for three types of NLC FP etalons having thicknesses of 30.6 μm, 55.4 μm, and 108.8 μm. The Freedericksz transition voltages in the three cases are nearly equal. The measured effective refractive indices in the three cases decreased from 1.67 to 1.51 as the applied electric field intensity was increased. Beyond the threshold electric field, the effective refractive indices quickly decreased and eventually saturated at a value of 1.51 for all cases.

Keywords : Nematic liquid crystal, Refractive index, Wavelength-swept laser, Fabry-Perot etalon
OCIS codes : (060.2300) Fiber measurements; (060.2370) Fiber optics sensors; (140.3510) Lasers, fiber

I. INTRODUCTION

Liquid crystal (LC) materials have an effective refractive index which can be easily varied using thermal, electric, and magnetic fields. Therefore, optical-fiber sensors based on LC devices [1-3] have attracted attention in the electric power industry as devices to measure the electro-magnetic field. There are several optical-fiber sensors using the LC devices, such as an LC infiltrated photonic crystal fiber, an LC tunable fiber polarizer, an LC film, and a Fabry-Perot (FP) etalon with an LC [4-8]. In particular, an FP etalon with an LC [7, 8] has advantages such as simple structure, high finesse, and low-voltage drive. The LC in the FP etalon is used as an active medium that can be controlled by changing the applied voltage. Therefore, it can be used as a wavelength-tunable filter. Several nematic LC (NLC) FP tunable filters have been reported in various configurations [8-10]. When the NLC in the FP etalon is homogeneously aligned between alignment layers, the alignment of the NLC directors is gradually reoriented according to the applied electric-field intensity [3]. It is very important to measure the effective refractive index of the LC for use as a sensing device. In this study, we measure the effective refractive index of the NLC inside the FP etalon according to the applied electric fields by using the wide-band wavelength-swept laser (WSL) with a polygon-scanner-based wavelength filter. We fabricate three types of NLC FP etalons having thicknesses of 30.6 μm, 55.4 μm, and 108.8 μm. For each case, the Freedericksz transition voltages are measured. The effective refractive index of the NLC depends on the applied static-electric-field intensity.

II. THEORY

The FP etalon is the most commonly used device for producing a large number of mutually coherent beams by dividing the amplitude. Figure 1 shows a schematic of a simple case of the FP etalon. Even though the mirrors are flat and parallel, there are losses due to scattering or absorption

*Corresponding author: myjeon@cnu.ac.kr
Color versions of one or more of the figures in this paper are available online.

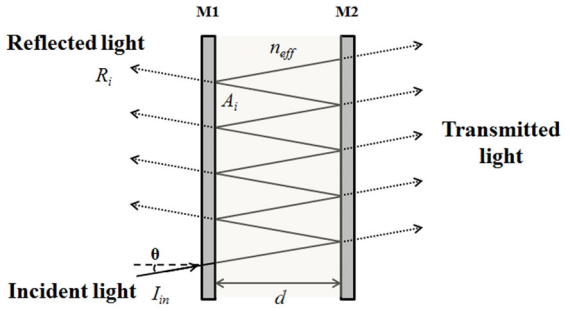

FIG. 1. Fabry-Perot etalon; A_i denotes absorption and R_i denotes reflection.

in the mirror. In this study, we will consider only normal incidence to the FP etalon. Inside the FP etalon, which consists of two parallel and partially reflecting surfaces, the incident beam is innumerably reflected and multiple transmitted beams interfere.

The optical path difference between any two successive transmitted rays is $2n_{eff}dcos\theta$, where d is the separation between the two reflecting surfaces, n_{eff} is the effective refractive index of the material between the reflecting surfaces, and θ is the incident angle with respect to the surface normal. In this case, the incident angle $\theta = 0°$ is assumed. The transmitted rays have different phases and intensities with respect to the adjacent ray. When light with an intensity of I_{in} is incident on the mirror surface, the intensity is partly transmitted because of reflection on the surface and absorption in the mirror. The phase difference δ originating from the optical path difference is given by

$$\delta = 2kd = \frac{4\pi}{\lambda_0} n_{eff} d \tag{1}$$

where λ_o is the wavelength in free space. Thus, the condition for the appearance of a maximum fringe of the FP etalon is given by

$$2m\pi = \frac{4\pi}{\lambda_m} n_{eff} d \tag{2}$$

where m denotes the order number of interference and λ_m is the m-th wavelength of the transmission peak. Therefore, the m-th and (m+1)-th wavelengths ($\lambda_m > \lambda_{m+1}$) of the two consecutive wavelengths are given by

$$\lambda_m = \frac{2n_{eff}d}{m}, \quad \lambda_{m+1} = \frac{2n_{eff}d}{m+1} \tag{3}$$

The effective refractive index is calculated from Eq. (3) as follows:

$$n_{eff} = \frac{1}{2d}\left[\frac{\lambda_m \lambda_{m+1}}{\lambda_m - \lambda_{m+1}}\right] \tag{4}$$

The effective refractive index can be estimated by measuring two consecutive wavelengths.

III. NEMATIC LIQUID CRYSTAL FABRY-PEROT ETALON

The commercially available 4-cyano-4'-pentylbiphenyl (5CB, from Merck) is used as the NLC. This compound exhibits nematic-phase properties in the temperature range of 24℃ to 36℃. In order to measure the effective refractive index of the NLC, an FP etalon with NLC is fabricated. The cell structure of the fabricated NLC FP etalon is shown in Fig. 2. It consists of glass substrates, gold layers, polyimide layers, and an NLC layer. The gold layers, having highly reflective surfaces, are deposited on the glass substrates and are used as the electrodes. The gold layers cause high optical loss owing to their high reflectance and absorption. To reduce this optical loss, they can be fabricated with dielectric materials and indium tin oxide [11]. The polyimide layers function as planar alignment layers and are deposited on the gold layers and rubbed for the alignment of NLC molecules along the surfaces.

The NLC is homogeneously aligned between the polyimide layers. The thickness of the gold layer is approximately 30 nm. The NLC is aligned parallel to the polyimide layers (x-axis) in the absence of an electric field. The electric field is applied between the gold layers along the z-axis. Therefore, the director is gradually reoriented along this axis as the electric field intensity increases. The NLC is a birefringent material, which has two refractive indices; n_o (ordinary refractive index) in the ordinary mode and n_e

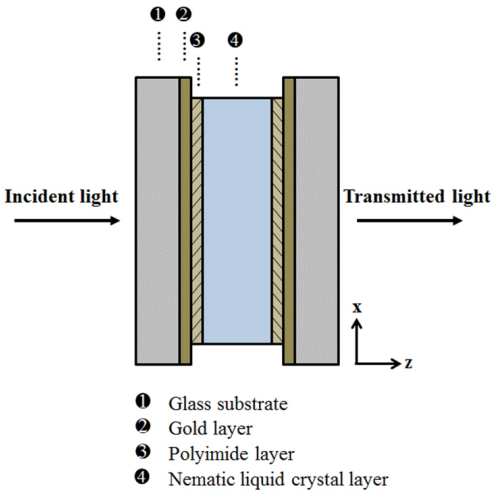

FIG. 2. Structure of the nematic-liquid-crystal Fabry-Perot etalon.

(extraordinary index) in the extraordinary mode [8].

The polarization of the input beam can be controlled in the direction of the extraordinary mode. Then, there only exists the extraordinary mode of the transmitted peaks from the NLC FP etalon [3]. In the experiments, we fabricated three types of FP etalons having thicknesses of 30.6 μm, 55.4 μm, and 108.8 μm. The reflectivity of the gold layer and insertion loss of the NLC FP etalon are ~ 90% and ~ 20 dB, respectively.

IV. EXPERIMENTS

Figure 3 shows the experimental setup for measurement of the effective refractive index variation of the NLC with respect to the applied electric field. The setup consists of a WSL, an NLC FP etalon, and a linear polarizer. The wide-band, high-power WSL incorporating a polygon-scanner-based wavelength filter is used as a broadband optical source. It comprises two semiconductor optical amplifiers (SOAs), two polarization controllers, an optical circulator, an optical output coupler, and a polygon-scanner-based wavelength filter. The bandwidth of the WSL is greater than that of the ASE from the SOA. The dotted box in the figure represents the polygon-scanner-based wavelength filter, which consists of a polygon rotating mirror, a diffraction grating, and two achromatic doublet lenses [12].

Since the NLC FP etalon has high insertion loss, two SOAs are used to improve the output power of the WSL [13]. The center wavelength of the WSL is approximately 1310 nm, and the output power is greater than 20 mW. The 3 dB bandwidth of the WSL is greater than 90 nm. The collimated output beam of the WSL is launched into the NLC FP etalon through a linear polarizer. External electric fields are applied to the NLC FP etalon by using an arbitrary function generator (Tabor Electronics Inc., 8023). The applied voltage has a square waveform with 10-kHz AC voltage to protect the material from electrolytic disruption [14]. The output of the NLC FP etalon is collected using a collimator and measured with an optical spectrum analyzer while the applied voltage is gradually increased from 0 to 9 V. In the experiments, the applied voltages are converted to the applied electric fields according to the thickness of the NLC cell because it is more appropriate to discuss the results in terms of voltages per unit thickness.

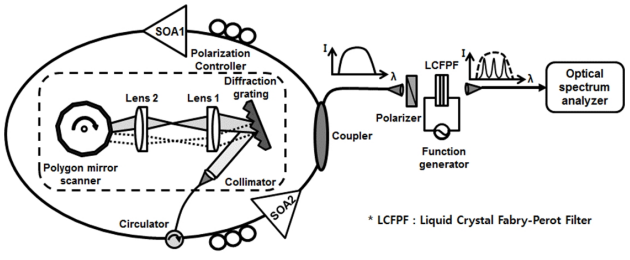

FIG. 3. Experimental setup for measuring the variation in the effective refractive index of the NLC according to the applied electric field.

V. RESULTS AND DISCUSSION

Figure 4 (a) shows the optical spectrum of the transmitted output from the NLC FP etalon of thickness 30.6 μm. The effective refractive index can be estimated by selecting two arbitrary consecutive wavelengths of the transmitted peaks. Figure 4 (b) shows a plot of the effective refractive index of the NLC as a function of the static applied electric field for the 30.6-μm-thick etalon. Under the threshold voltage corresponding to the Freedericksz transition voltage [15], the effective refractive index does not change with the applied electric field. Above the threshold voltage, however, the LC directors rotate because of the force balanced between the elastic restoring force and the torque of the induced dipole moment caused by the external electric field as the applied electric field increases. The Freedericksz transition voltage was approximately 0.77 V_{rms} for the 30.6-μm-thick NLC FP etalon. The threshold value of the electric field corresponding to the Freedericksz transition was approximately 25.0 mV/μm. For electric fields greater than ~150

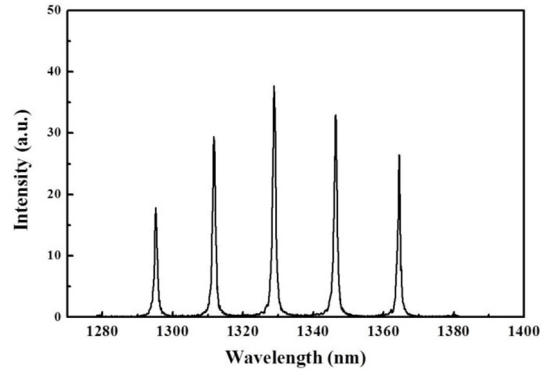

(a)

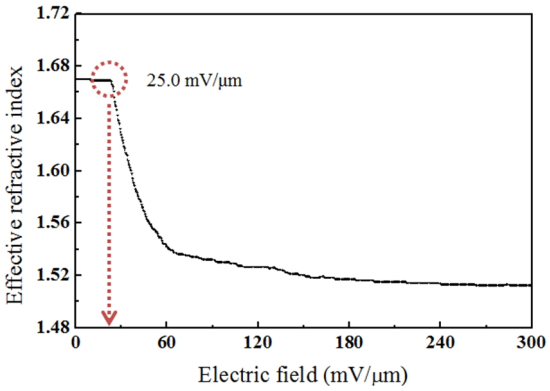

(b)

FIG. 4. (a) Optical spectrum of the transmitted output from the NLC FP etalon of thickness 30.6 μm; (b) effective refractive index of the NLC as a function of the applied electric field for the 30.6-μm-thick etalon.

mV/μm, the effective refractive index gradually saturated.

Figure 5 (a) and 6 (a) show the optical spectra of the transmitted output from the NLC FP etalons of thicknesses 55.4 μm and 108.8 μm, respectively. The peaks in Fig. 6 (a) are broader than those in Figs. 4 (a) and 5 (a) because of the misalignment of the NLC FP etalon. The interval between two arbitrary consecutive wavelengths decreases as the thickness of the NLC FP etalon increases. Figure 5 (b) and 6 (b) show plots of the effective refractive index of NLC as a function of the static applied electric field for 55.4-μm-thick and 108.8-μm-thick NLC FP etalons, respectively. The Freedericksz transition voltages for the 55.4-μm-thick and 108.8-μm-thick NLC FP etalons were approximately 0.78 V_{rms} and 0.90 V_{rms}, respectively; the threshold values of the electric fields corresponding to these Freedericksz transition voltages were approximately 14.1 mV/μm and 8.3 mV/μm, respectively. The effective refractive indices at electric fields greater than 100 mV/μm and 50 mV/μm gradually saturated for 55.4-μm-thick and 108.8-μm-thick etalons, respectively, as shown in Fig. 5 (b) and Fig. 6 (b). The effective refractive indices of the NLC for the three fabricated NLC FP etalons remain at approximately 1.67 until the threshold electric fields are reached. On the other hand, beyond the threshold electric field, the effective refractive indices quickly decrease and eventually saturate at a value of 1.51 for all cases. The measured Freedericksz transition voltages were nearly equal for the 30.6-μm-thick and 55.4-μm-thick NLC FP etalons. However, the measured Freedericksz transition voltage of the 108.8-μm-thick etalon was slightly higher than those of 30.6-μm-thick and 55.4-μm-thick etalons. The reason is that the directors require more time to stabilize inside the FP etalon for the 108.8-μm-thick NLC FP etalon.

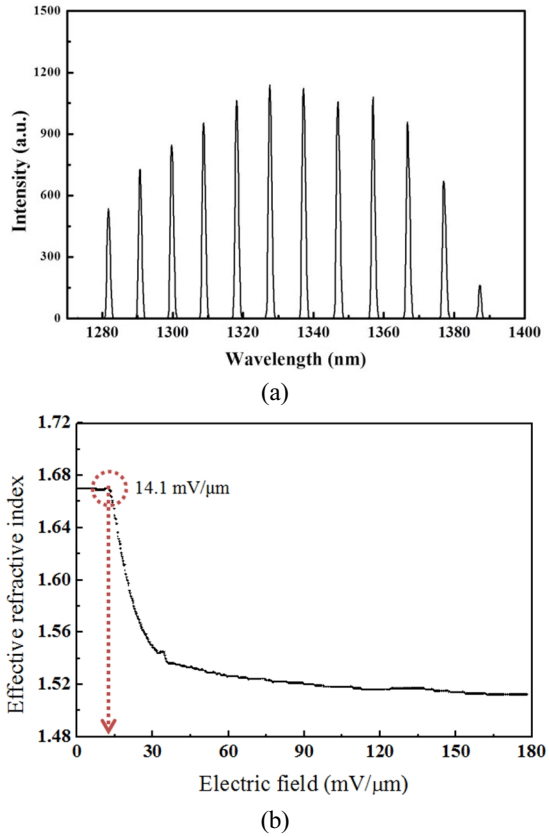

FIG. 5. (a) Optical spectrum of the transmitted output from the NLC FP etalon of thickness 55.4 μm; (b) effective refractive index of the NLC as a function of the applied electric field for the 55.4-μm-thick etalon.

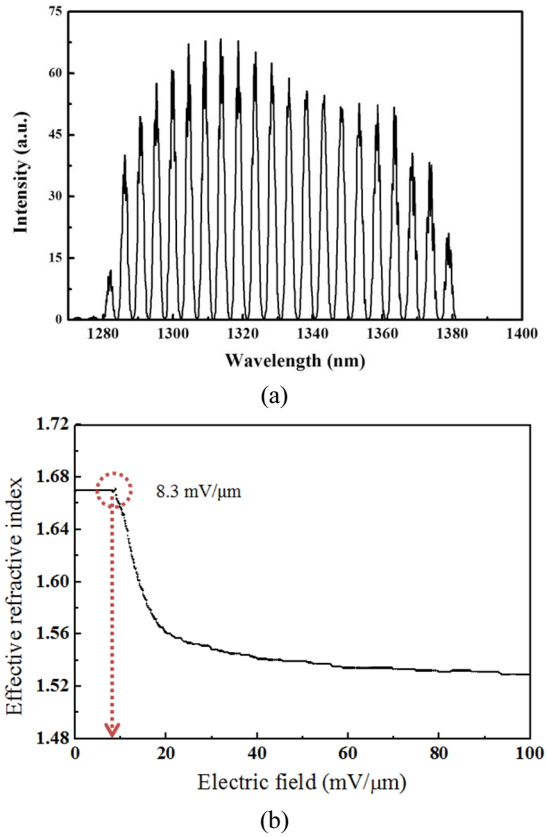

FIG. 6. (a) Optical spectrum of the transmitted output from the NLC FP etalon of thickness 108.8 μm; (b) effective refractive index of the NLC as a function of the applied electric field for the 108.8-μm-thick etalon.

VI. CONCLUSION

We successfully measured the effective refractive index of a nematic liquid crystal (NLC) in a Fabry-Perot (FP) etalon according to the applied electric field by selecting two arbitrary consecutive wavelengths of the transmitted peaks. A wide-band, high-power, wavelength-swept laser is used as an optical source to measure the transmitted peaks of the NLC FP etalons. We measured the Freedericksz transition voltages for three types of the NLC FP etalons having thicknesses of 30.6 μm, 55.4 μm, and 108.8 μm. The Freedericksz transition voltages were nearly equal in all three cases. However, the threshold value of the electric

field corresponding to the Freedericksz transition voltages decreased as the thickness of the NLC FP etalons was increased. The measured effective refractive indices in the three cases decreased from 1.67 to 1.51 as the applied electric field was increased.

ACKNOWLEDGMENT

This work was supported by the Human Resource Training Progran for Regional Innovation through the Ministry of Education and National Research Foundation of Korea (NRF-2013H1B8A2032213) and by Basic Science Research Program through the National Research Foundation of Korea (NRF) funded by the Ministry of Science, ICT and Future Planning (NRF-2014R1A2A1A11051152)

REFERENCES

1. M. Tabib-Azar, B. Sutapun, T. Srikhirin, J. Lando, and G. Adamovsky, "Fiber optic electric field sensors using polymer-dispersed liquid crystal coatings and evanescent field interactions," Sens. Actuators A **84**, 134-139 (2000).
2. S. Mathews, G. Farrell, and Y. Semenova, "Liquid crystal infiltrated photonic crystal fibers for electric field intensity measurements," Appl. Opt. **50**, 2628-2635 (2011).
3. M. O. Ko, S.-J. Kim, J.-H. Kim, B. W. Lee, and M. Y. Jeon, "Dynamic measurement for electric field sensor based on wavelength-swept laser," Opt. Express **22**, 16139-16147 (2014).
4. T. T. Larsen, A. Bjarklev, D. S. Hermann, and J. Broeng, "Optical devices based on liquid crystal photonic bandgap fibres," Opt. Express **11**, 2589-2596 (2003).
5. L. R. Jaroszewicz, S. J. Kłosowicz, K. Czupryński, A. Kiezun, E. Nowinowski-kruszelnicki, and T. Niedziela, "Tunable liquid crystal fiber-optic polarizer and related elements," Molecular Crystals and Liquid Crystals Science and Technology, Section A. Molecular Crystals and Liquid Crystals **368**, 17-24 (2006).
6. H.-R. Kim, E. Jang, and S.-D. Lee, "Electrooptic temperature sensor based on a Fabry-Pérot resonator with a liquid crystal film," IEEE Photon. Technol. Lett. **18**, 905-907 (2006).
7. Y. Bao, A. Sneh, K. Hsu, K. M. Johnson, J.-Y. Liu, C. M. Miller, Y. Monta, and M. B. McClain, "High-speed liquid crystal fiber Fabry-Perot tunable filter," IEEE Photon. Technol. Lett. **8**, 1190-1192 (1996).
8. J.-H. Lee, H.-R. Kim, and S.-D. Lee, "Polarization-insensitive wavelength selection in an axially symmetric liquid-crystal Fabry-Perot filter," Appl. Phys. Lett. **75**, 859-861 (1999).
9. J. S. Patel and S.-D. Lee, "Electrically tunable and polarization insensitive Fabry-Perot etalon with a liquid-crystal film," Appl. Phys. Lett. **58**, 2491-2493 (1991).
10. K.-C. Lin and W.-C. Chuang, "Polarization-independent and electronically tunable Fabry-Perot etalons with cross-orthogonal liquid-crystal layers," Microwave Opt. Technol. Lett. **38**, 475-477 (2003).
11. I. Abdulhalim, "Optimized guided mode resonant structure as thermooptic sensor and liquid crystal tunable filter," Chin. Opt. Lett. **7**, 667-670 (2009).
12. Y. S. Kwon, M. O. Ko, M. S. Jung, I. G. Park, N. Kim, S.-P. Han, H.-C. Ryu, K. H. Park, and M. Y. Jeon, "Dynamic sensor interrogation using wavelength-swept laser with a polygon-scanner-based wavelength filter," Sensors **13**, 9669-9678 (2013).
13. M. O. Ko, N. Kim, S.-P. Han, K. H. Park, B. W. Lee, and M. Y. Jeon, "Characteristics of a wavelength-swept laser with a polygon-based wavelength scanning filter," Korean J. Opt. Photon. (Hankook Kwanghak Hoeji) **25**, 61-66 (2014).
14. W. Vogel and M. Berroth, "Tunable liquid crystal Fabry-Perot filters," Proc. SPIE **4944**, 293-304 (2002).
15. P. G. de Gennes and J. Prost, *The Physics of Liquid Crystals* (Clarendon Press, Oxford, USA, 1993), Chapter 3.